Indian Journal of Engineering & Materials Sciences
Vol. 11, August 2004, pp. 276-282

Complex characterization of physiology solution based magnetic fluid[†]

M Timko[a], M Koneracká[a], P Kopčanský[a], Z Tomori[a], L Vékas[b], A Józefczak[c], A Skumiel[c], A Radenovic[d], G Dietler[d], E Bystrenová[a,d] & M Lita[e]

[a]Institute of Experimental Physics of Slovak Academy of Sciences, Košice, Slovakia
[b]Centre for Fundamental and Advanced Technical Research of Romanian Academy, Timisoara, Romania
[c]Institute of Acoustics, Adam Mickiewicz University, Umultowska 85, Poznan, Poland
[d]IPMC Université de Laussane, CH-1015 Laussane, Switzerland
[e] University POLITEHNICA Timisoara,Timisoara, Romania

Received 24 January 2003; accepted 5 December 2003

Atomic force microscopy (AFM), transmission electron microscopy (TEM) and magnetization measurements by vibrating sample magnetometer (VSM) were used for estimation and comparison of size of magnetite particles in physiology solution based magnetic fluid (MF). The mean particle diameter values were 7.6 nm, 9.3 nm and 10.6 obtained by AFM, VSM and TEM, respectively. For the analysis of AFM pictures the more precise method was developed where the particle size was calculated as the geometrical mean of sizes in all three dimensions. The structural stability of prepared MF was affirmed by the ultrasonic measurements.

IPC Code: Int. Cl.[7] H01F 1/44

The physical and chemical properties of magnetic fluids (MF) are strongly influenced by the details of the distribution in size and shape of the dispersed colloidal magnetic nanoparticles. Magnetic measurements (VSM) and transmission electron microscopy (TEM) have been traditionally used to obtain the particle size profile of their nanometer dimensions. Only recently has atomic force microscopy (AFM) been used to image magnetic nanoparticles dispersed within MF[1,2]. The main application of AFM is high resolution imaging of different material surfaces including metals[3], polymers[4], ceramics[5], biomolecules[6] and cells[7]. The unique resolution of most AFM techniques is based on the ultra-sharp AFM probes (tips with radii of typically 4-60 nm) attached to a flexible cantilever and accurate ceramic piezoelements which allow the sample to be scanned in the x-y plane with sub-nanometre precision. The piezoelements move in z-direction, for example to maintain a constant force between the probe and the sample. The AFM tip scans over the sample surface and the AFM records interaction between the tip and the surface is recorded, providing a high-resolution topographic image[8]. In this paper, we report a newly developed method of sample preparation that allows reliable AFM imaging of nanometer-sized, nearly spherical magnetite particles originally dispersed within a MF. The particle size is calculated as the geometrical mean of sizes in all 3 dimensions (x,y,z). The z-size is determined as a difference between the average background level and the top of particle, the x and y sizes are determined as a Feret diameter of particle outline measured in one half of height. Also, the particle size histogram obtained from the AFM image data is compared with the particle size histogram obtained from TEM and VSM measurement data. The physiological solution based MF has been studied by ultrasonic methods. The ultrasonic wave propagation velocity and absorption coefficient were measured as a function of temperature for different values and geometries of magnetic field.

Materials and Methods

Sample preparation and measurements

The MF used in this experiment was obtained by chemical precipitation of a mixture of ferric and ferrous salts in an alkaline aqueous medium. The stabilization of the magnetite precipitate in a physiology solution (9 wt% NaCl aqueous solution) was achieved by surface coating the magnetite nanoparticles with sodium oleate.

[†]Presented at International Workshop on Recent Advances in Nanotechnology of Magnetic Fluids, held at National Physical Laboratory, New Delhi, during 22-24 January 2003

The preparation of the magnetite nanoparticles for AFM imaging was done by De Rose and Revel method[9]: The stock colloidal suspension of magnetic particles was diluted to a concentration around 10 billion (10^{10}) particles/mL (a dilution of about 10^4 times) into a buffer solution ($7 \leq p\text{H} < 8$). The diluted sample of MF was centrifuged at 15, 000 rpm in a small microfuge tube in fixed angle rotor for 60-75 min. After several washings and subsequent centrifugations a small volume of solution was pipetted out and was allowed to dry onto a freshly cleaved mica surface (10 mm×10 mm) in the air. From the AFM images, a population of about 60 particles was analysed.

The imaging and measurement of the particles were done using a Nanoscope IIIa Multimode SPM (Digital Instruments, Santa Barbara, CA) and its image analysis software as well as with the own software. The particles were imaged in tapping mode at a scan rate between 1 and 3 Hz and a set point voltage of 1-2 V using rectangular silicon (Si) cantilevers/probes (Nanosensors, Wetzlar-Blankenfeld, Germany) with a resonant frequency of about 300 kHz[9].

Examination of the nanosized magnetic particles by TEM was done using a Tesla BS 500 microscope normally operated at 90 kV and 80, 000 × magnification by replication technique. A drop of magnetic fluid sample containing 5×10^{14} particle/cm^3 was deposited on the 400 mesh copper grid and air dried before the picture was taken. About 1420 particles were analysed in the TEM image data.

The magnetization measurements of the studied MF were carried out with a VSM magnetometer. The ultrasonic wave propagation velocity and absorption coefficient were measured as a function of temperature for different values of magnetic field. The propagation velocity was measured by the echo-overlap method proposed by Papadakis[10], while the changes in the absorption coefficient by the pulse method on the MATEC apparatus[11].

Method of AFM image analysis

The principle of AFM is based on the mechanical contact between the sample and tip. Measurement of particles in nanometer scale is therefore strongly affected by the tip-sample interaction. This interaction during the scan in (x-y) directions is usually expressed as a convolution of the tip and the sample shapes. Although built-in functions of AFM can partly eliminate this effect, the error of a measurement increases with growing resolution. Another approach to particle size measurement is based on the determination of its height from the brightness difference using calibration strip, which shows relation between the colour and the height. Although the tip effect in z-direction is minimal, substantial influence has the pressure of the tip.

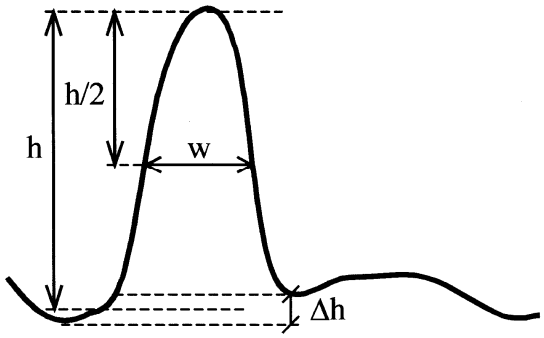

Fig.1—Graph representing cross-section of particle. Peak height (*h*) is calculated as the difference between the average background level and the peak top. Peak width (*w*) is measured in one half of the height.

To achieve the most objective result, measurements in both: horizontal (x-y) and vertical (z) directions are usually combined. Fig. 1 represents one-dimensional "cross-section" of a particle. Program Nanoscope supplied with AFM microscope offers such interactive cross-section function to measure particle size by following manner: (i) Draw a line representing cross-section in x-direction through the selected particle on an AFM image. As a result a graph like this on Fig. 1 appears. (ii) Find the background level as an average of minimal values on both sides of peak. Measure the distance *h* (height) between the background and the peak top. Resulting height represents the z-direction size S_z. (iii) Find the peak width *w* measured in one half of the height. Resulting value represents S_x. (iv) Draw a cross-section line in y-direction and repeat the measurement to obtain S_y. (v) Calculate resulting size as the geometrical mean $S = (S_x\, S_y\, S_z)^{1/3}$

Improved method of particles analysis based on active contours

The cross-section method shown on Fig. 1 respects the topological nature of AFM image and is built in the software supplied with AFM microscope However, cross-section is not very objective as it assumes that human operator draws a line cutting the analyzed particle and therefore it is dependent on the operator's subjective choice. In addition to it, analysis requiring human interaction is very time-consuming.

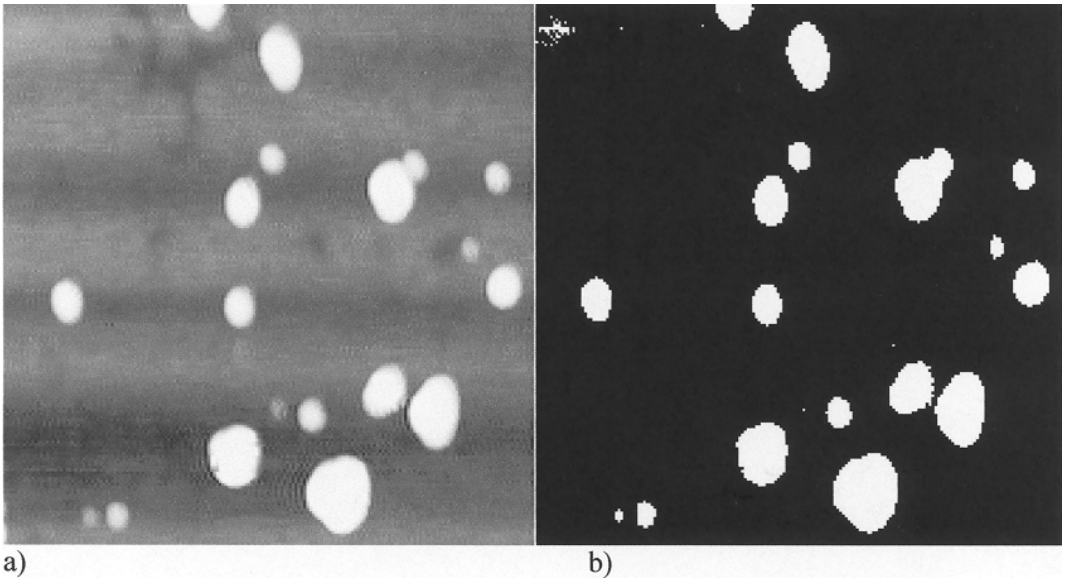

Fig. 2—(a) Original image and (b) binary image achieved by thresholding (right).

We developed own method respecting the philosophy described above, but eliminating mentioned disadvantages. In fact, our method is an extension of method shown on Fig. 1 into two-dimensional space. It is based on direct processing of AFM image and therefore cross-section line drawing is not required. Method consists of several steps performing particles detection and measurement:

Thresholding

Thresholding is the only step requiring human interaction, where the value of threshold T is set manually using the slider control. An input AFM image is shown in Fig. 2a. The result of thresholding is binary image (Fig. 2b) which displays with white color all pixels brighter than T and with black color the rest ones. White pixels create connected regions R_i, roughly corresponding to analyzed particles. Optimal T value is that which achieves the best match of regions and particles. However, single global value of T cannot always be optimal for the whole image and therefore programme offers the possibility to adjust individual thresholds for selected parts of an image.

The detection of edges

For each connected region R_i, closed curve L_i is found which encloses all pixels of region R_i. Curve L_i is defined as the succession of points P_j given by (x_i,y_i) coordinates. L_i usually consists of pixels with maximal gradient that are easily detectable by the human visual system. The edges (contours) detected in this step are visible on Fig. 3a. Edges found in this step define individual particles that will be subjects of further processing and measurement. However, some objects are not proper for further processing (e.g. touching clusters of particles) and should be removed from the statistics. On the other hand, some objects were not detected by thresholding. In both cases, program allows manual addition or removing of wrongly detected outlines.

Search from minimal background level

The results of edge detection represent an initial state of the optimization. Next, algorithm searches for pixels representing the position, where particle touches the background. The optimization is based on the model of active contour (snake), which tries to find local minimum, but it takes into account also the elasticity of contour. Thus algorithm searches for the minimal value of function:

$$g(W)=\frac{1}{L}\sum_i w_I \cdot f_I\left(P_i\right)+w_C f_C\left(P_i\right)+w_B f_B\left(P_i\right) \quad \ldots (1)$$

where $f_I(Pi)$ is image force, which pushes the curve to the low-intensity (darkest) parts of AFM images, $f_C(Pi)$ are internal forces which impose the regularity of the curve (elasticity and rigidity) and $f_B(Pi)$ is a force pushing curve inside. [For details concerning active contours (snakes)[12]].

The effect of active contour optimization can be seen on Fig. 3b, where two contours are visible. If the object edge is represented by maximal brightness gradient then outer contour displays the local

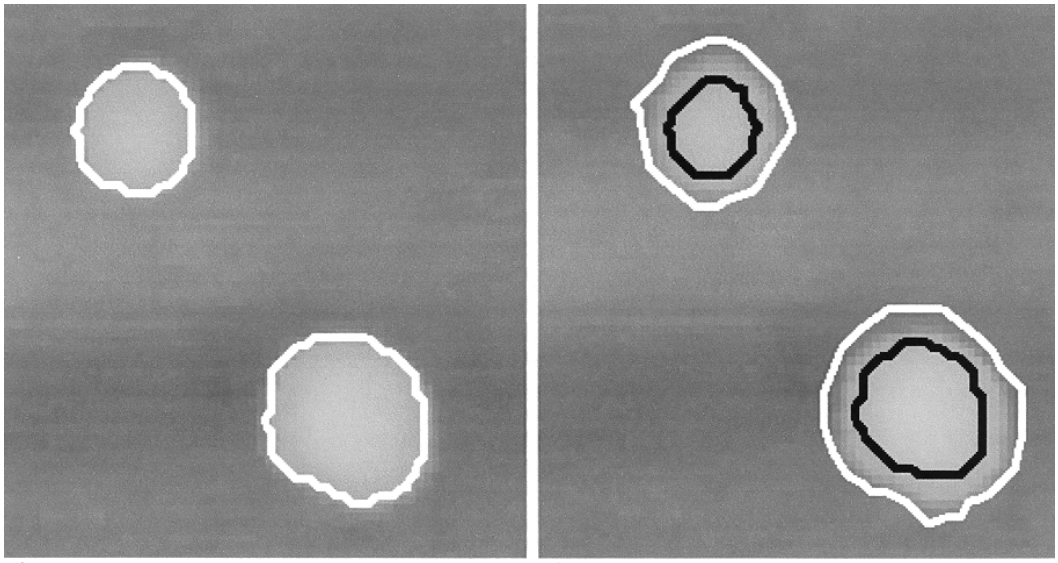

Fig. 3—(a) Initial (starting) shape of edges and (b) result of optimization is outer (white) border representing edge of particle near the background. Inner edge (black) is edge of particle measured in one half of height.

brightness minimum found near the edge. The inner contour represents the half value of brightness between base and top of object (see object cross-section in Fig. 1). Coefficients in Eq. (1) allow fine-tuning of the optimization (e.g. if the compact shape is emphasized).

Particle size calculation

Particle size calculation exploits the optimized contour found in previous stage. Initially, one representative value of background is calculated as an average value along the contour. Then the height of i^{th} particle is calculated as a difference between the average value of all L_i points and the gray level corresponding to the brightest point of region R_i. Then, threshold T is set equal to half height of particle. Thresholding and edge detection (steps 1 and 2) are applied on the close neighbourhood of particle. As a result, edge in one half of height is found (black outline on Fig. 3b). The diameter of this outline should be found. We exploited Feret diameter as the proper estimate of diameter. (Feret diameter of irregular 2D object is equal to the diameter of circle having the equal area).

The final value representing the particle diameter is calculated as the geometrical mean of sizes in all three dimension (x, y, z), where values in x and y directions are equal to the Feret diameter and z value is the height.

Method of AFM particles analysis using active contours has been implemented as a Windows program module "AFM Particles" written in Visual C++.

Results and Discussion

Fig. 4 presents temperature dependencies of the ultrasonic wave propagation velocity obtained for water and for the fluid studied, without a magnetic field. The propagation velocity in water changes as a parabolic function with a maximum at 74°C, in consistence with the Willard equation. As the magnetic fluid studied is based on a water solution of NaCl, the temperature changes in the ultrasonic wave propagation velocity in it also have a parabolic character. The lower velocity and a shift of the maximum towards lower temperatures is a result of the addition of NaCl, magnetic particles and surfactant, as it has been also established in our earlier study of the fluid EMG-605, based on water, produced by the Ferrofluid Corporation.

Figs 5a and 5b present the temperature dependencies of the ultrasonic wave propagation in the MF for different values of magnetic induction, and for two geometries $B \perp k$ and $B \parallel k$. A significant effect of an external magnetic field on the propagation velocity is evident. With increasing magnetic field the structure of the MF becomes increasingly rigid, causing an increase in the ultrasonic wave propagation velocity. At temperatures

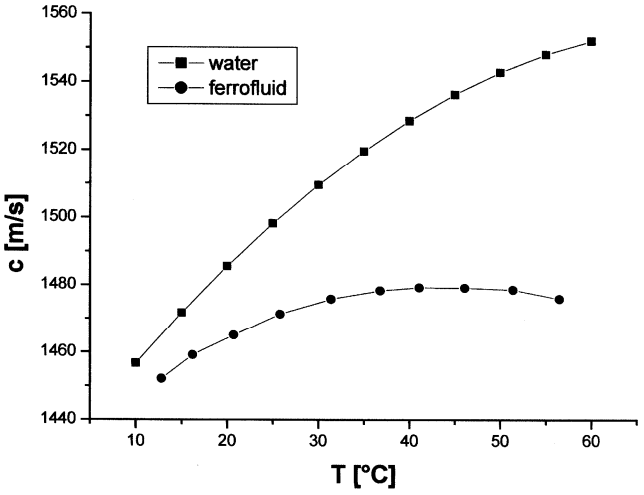

Fig. 4—Temperature dependencies of the ultrasonic wave propagation in water and the physiology solution based MF

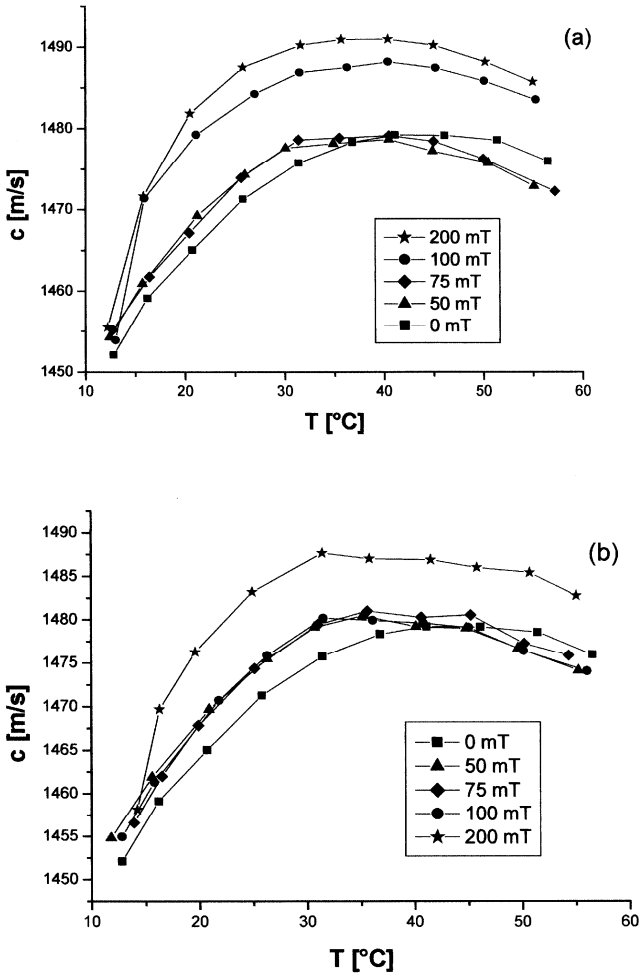

Fig. 5—Temperature dependence of the ultrasonic wave propagation velocity in the MF for a few different values of the magnetic field induction, for (a) $B \perp k$ and (b)$B \parallel k$

above 40°C, so after the maximum, the propagation velocity decreases faster in the field than without it, as it is easily seen for the lower field values 50 and 75 mT. Most probably it is a result of formation of clusters changing the conditions of the ultrasonic wave propagation. The appearance of clusters for higher temperatures has been confirmed by the changes in the absorption coefficient.

Figs 6a and 6b present the temperature dependencies of the ultrasonic wave absorption coefficient for different values of the magnetic field induction and for two geometries $B \perp k$ and $B \parallel k$. We can see that no changes of the absorption coefficient were observed in zero external magnetic field induction. It means that MF has a good structural

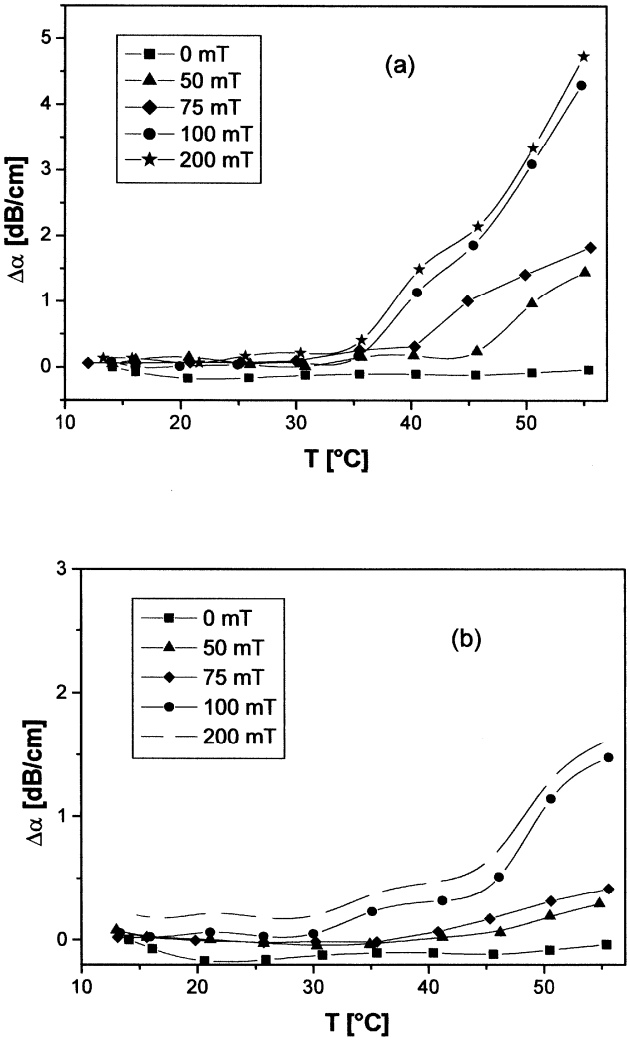

Fig. 6—Temperature dependence of the ultrasonic wave absorption coefficient for a few different values of the magnetic field induction, for (a) $B \perp k$ and (b)$B \parallel k$.

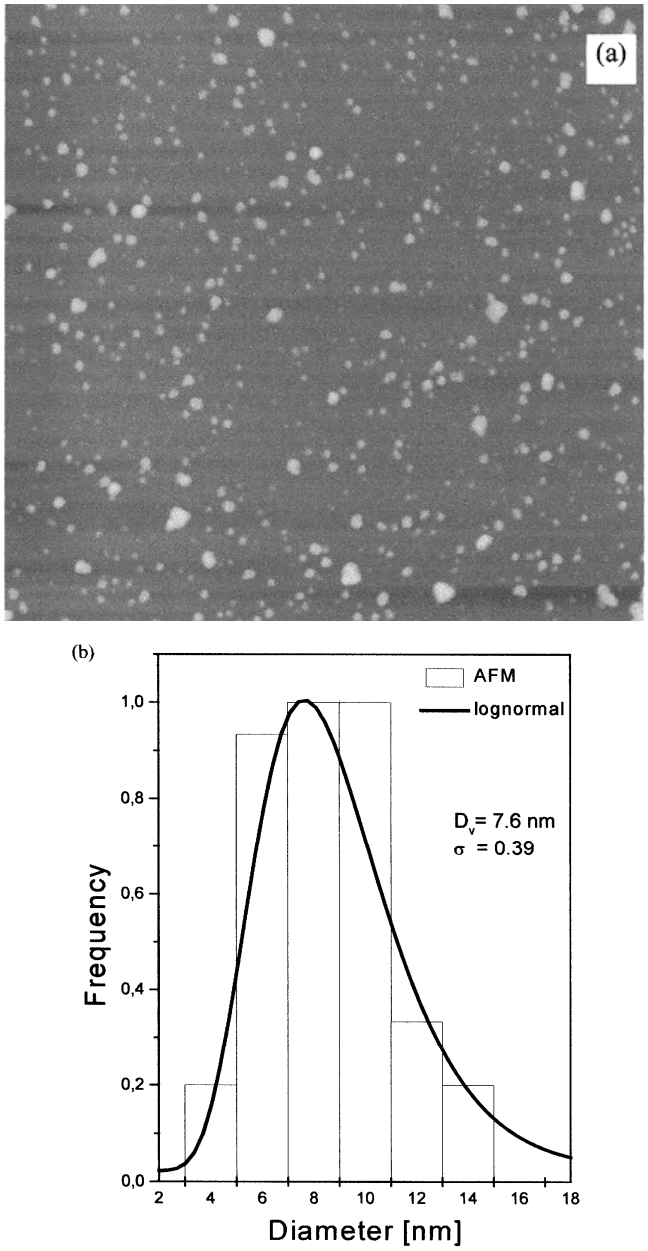

Fig. 7—AFM image of magnetite (a) nanoparticles and (b) relevant particle size histogram

stability. In low temperatures, up to about 35°C, the effect of the magnetic field induction on the absorption coefficient was rather insignificant, and its slight increase is probably a result of an increase in the MF viscosity with increasing magnetic field induction. For temperatures above 35°C the changes in the absorption coefficient are more pronounced and their magnitude is in direct proportion to the field. The magnitude of the changes in the absorption coefficient was observed to depend on the angle between the direction of the wave propagation and the lines of the external magnetic field. In the $B \perp k$ geometry the changes in the absorption coefficient were much greater than in the $B \parallel k$ geometry. These results suggest the formation of chain-like clusters in the ferrofluid studied in the range of temperatures above 35°C. The clusters are arranged along the lines of the external magnetic field – the ultrasonic wave propagation is greater along the chain clusters and for the geometry $B \parallel k$ the changes in $\Delta\alpha$ are smaller.

Fig. 7a shows the AFM image of nanosized magnetite particles taken from 1 × 1 μm. area at a scan rate of 1.498 Hz. The total area of the sample was approximately 10 × 10 mm^2. Several regions of the sample were imaged and analysis of the nanoparticles present within the areas scanned allowed us to make a histogram of the particle sizes measured (see Fig. 7b). Due to the fact that probe-sample convolution causes a dilation of the lateral dimensions, only the heights of the particles were measured and used for calculating the mean particle diameter. This approach assumes the particles are indeed spherical in shape, but a recent study of particle shape has shown that this assumption is reasonably accurate[4]. In Fig. 7b, the solid line represents the best curve fit of the particle size histogram using the standard log-normal distribution function[2] with D_v = 7.6 nm and σ =0.39.

Fig. 8a shows the TEM picture obtained from the magnetite nanoparticles, from which the profile of the particle size polydispersity was obtained. Fig. 8b shows the particle size histogram obtained from the TEM data. The solid line represents the best curve fit of the particle size histogram again using the standard log-normal distribution function with D_v = 10.6 nm and σ = 0.22.

The saturation magnetization I_s was measured to be 14 mT. By the method of Chantrell *et al.*[13], the lognormal parameters of the particle size distribution have been calculated to be: mean particle diameter D_v, of 9.3 nm, and standard deviation σ, of 0.29.

From the results obtained by the various measurement techniques, it is clear that for the mean particle diameter values: $D_{v/AFM}$ (7.6 nm) <$D_{v/VSM}$ (9.3 nm) < $D_{v/TEM}$ (10.6 nm) and for the standard deviation values: σ_{AFM} (0.39) > σ_{VSM} (0.29) > σ_{TEM} (0.22). However, the smaller mean particle diameter observed from VSM data (9.3 nm) in comparison with value obtained from TEM data (10.6 nm) can be explained by the presence of a nonmagnetic surface layer around the magnetite particles. On the other

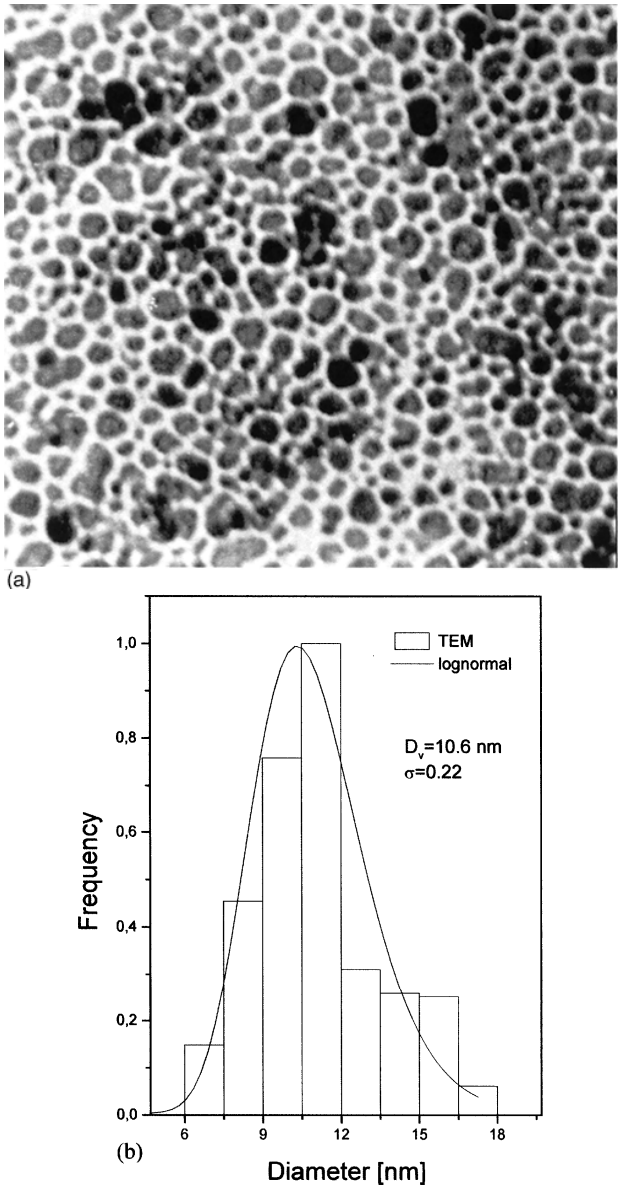

Fig. 8—Typical TEM picture (white line represents 20 nm) of magnetite (a) nanoparticles and (b) relevant particle size histogram

hand, the mean particle diameter obtained from AFM (7.6 nm) is reduced with to the TEM data by a factor 1.39. This difference may be caused by fact that the sample used for AFM experiment is very diluted in comparison with sample used in TEM experiment. So particle agglomeration can exist and sometimes is unable to clearly differentiate between agglomerates and particles.

Conclusions

This paper provides useful information concerning the particle size distribution and more precise method for analyzing of AFM images. The results from the ultrasonic wave propagation velocity and absorption coefficient revealed good structural stability of prepared MF in whole temperature interval of measurement. The application of external magnetic field changed then condition of stability and in temperatures above 35°C, the structure of this magnetic fluid has been observed to change with the magnetic particles forming chain-like clusters arranged along the lines of an external magnetic field.

Acknowledgement

This work was done under the auspices of the Slovak Academy of Sciences (grants No 3199 and 4068), Governmental programme SO 51/03R 06 00/03R 06 04, NATO project No.LST. CLG.977500 and KBN Research Grant No.8T07B 02720.

References

1 Bui Q T, Pankhurst Q A & Zulqar-main K, *IEEE Trans Magn,* 34 (1998) 2127.
2 Lacava B M, Azevedo R B, Silva L P, Lacava ZG M, Skeff Neto K, Buske N, Bakuzis A F & Morais P C, *Appl Phys Lett,*. 77 (2000) 1876.
3 Orisaka S, Minobe T, Uchihashi T, Sugawara Y & Morita S, *Appl Surf Sci,* 140 (1999) 243.
4 Jandt K D, McMaster T J, Miles M J & Petermann J, *Macomolecules,* 26 (1993) 6552
5 Baretzky B, Reinsch B, Taffner U, Schneider G & Ryhle M, *Z. Metallkunde,* 87 (1996) 332.
6 Klinov D V, Lagutina I V, Prokorov V V, Neretina T, Khil P P, Lebedev Y B, Chereny D I, Demin V V & Sverdlov E D, *Nucleic Acids Res,* 26 (1998) 4603.
7 DeRose J A & Revel J P, *Thin Solid Film,* 331 (1998) 194.
8 Binning G, Quate C F & Gerber C, *Phys. Rev. Lett*, 56 (1986) 930. DeRose J A & Revel J P, *J Microsc,* 195 (1999) 64.
9 Papadakis E P, *J Acoust Soc Am*, 42 (1967) 1045.
10 Skumiel A, Łabowski M & Hornowski T, *J Phys D: Appl Phys,* 30 (1997) 25.
11 Williams D J & Shah M, *Computer Vision, Graphics Image Process– Image Understand,* 55 (1992),14-26
12 Chantrell R W, Popplewell J & Charles S W, *IEEE Trans Magn,* 14 (1978) 975.